

Deep Sketch-Based Modeling of Man-Made Shapes

DMITRIY SMIRNOV, Massachusetts Institute of Technology

MIKHAIL BESSMELTSEV, Université de Montréal

JUSTIN SOLOMON, Massachusetts Institute of Technology

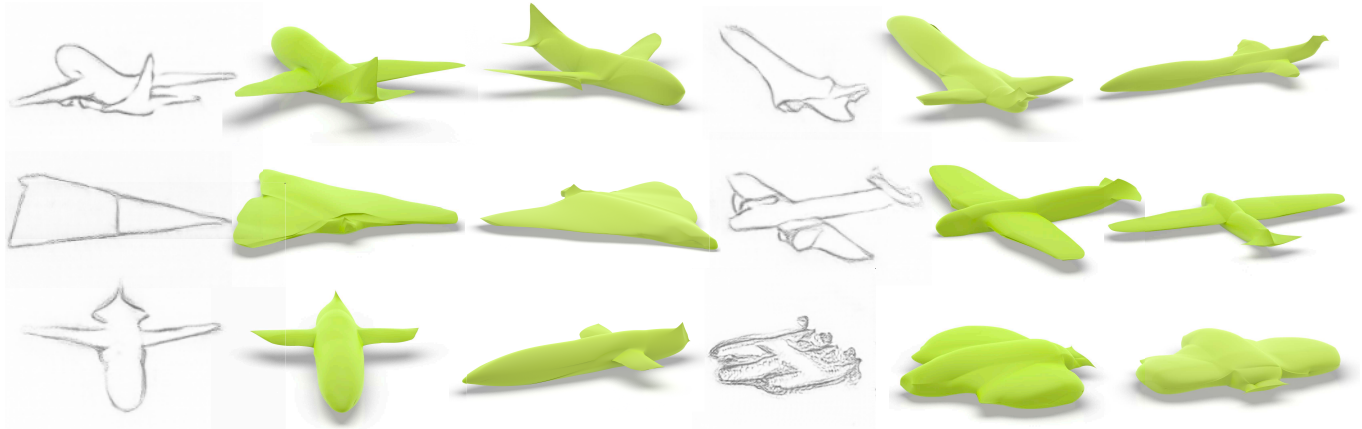


Fig. 1. Given a bitmap sketch of a man-made shape, our method automatically infers a complete *parametric* 3D model, ready to be edited, rendered, or converted to a mesh. Compared to conventional methods, our resolution-independent geometry representation allows us to faithfully reconstruct sharp features (wing and tail edges) as well as smooth regions. Results are shown on sketches from a test dataset. Sketches in this figure are upsampled from the actual images used as input to our method.

Sketch-based modeling aims to model 3D geometry using a concise and easy to create—but extremely ambiguous—input: artist sketches. Most conventional sketch-based modeling systems target smooth shapes and, to counter the ambiguity, put manually-designed priors on the 3D shape; they also typically require clean, vectorized input. Recent approaches attempt to learn those priors from data but often produce low-quality output. Focusing on piecewise-smooth man-made shapes, we address these issues by presenting a deep learning-based system to infer a complete man-made 3D shape from a single bitmap sketch. Given a sketch, our system infers a set of parametric surfaces that realize the drawing in 3D. To capture the piecewise smooth geometry of man-made shapes, we learn a special shape representation—a deformable parametric template composed of Coons patches. Naïvely training such a system, however, would suffer from lack of data and from self-intersections of the parametric surfaces. To address this, we introduce a synthetic sketch augmentation pipeline as well as a loss function that biases the network to output non-self-intersecting shapes. We demonstrate the efficacy of our system on a gallery of synthetic and real artist sketches as well as via comparison to related work.

CCS Concepts: • **Computing methodologies** → **Parametric curve and surface models**.

Additional Key Words and Phrases: Sketch-based Modeling, Deep Learning

Authors' addresses: Dmitriy SmirnovMassachusetts Institute of Technology; Mikhail BessmeltsevUniversité de Montréal; Justin SolomonMassachusetts Institute of Technology.

© 2019 Copyright held by the owner/author(s). Publication rights licensed to ACM. This is the author's version of the work. It is posted here for your personal use. Not for redistribution. The definitive Version of Record was published in *ACM Transactions on Graphics*, https://doi.org/0000001.0000001_2.

ACM Reference Format:

Dmitriy Smirnov, Mikhail Bessmeltsev, and Justin Solomon. 2019. Deep Sketch-Based Modeling of Man-Made Shapes. *ACM Trans. Graph.* 0, 0, Article 0 (2019), 12 pages. https://doi.org/0000001.0000001_2

1 INTRODUCTION

Algorithmically interpreting natural sketches as well as humans do would make 3D modeling intuitive and accessible. This is the goal of sketch-based 3D modeling research: to bring 3D modeling interfaces closer to paper-and-pencil sketching, allowing non-experts to quickly create expressive 3D content.

The task of interpreting a natural sketch and creating a 3D model automatically, however, remains unsolved. Converting rough, incomplete 2D input into a clean, complete 3D shape is extremely ill-posed, requiring inference of missing parts and interpretation of noisy sketch curves. To cope with these ambiguities, most systems rely on hand-designed shape priors. This approach severely limits the applications of those methods. Each shape category requires its own expert-designed prior, and many shape categories do not admit obvious means of regularizing the reconstruction process. A few recent papers explore the possibility of learning the shapes from data, implicitly learning the shape priors [Delanoy et al. 2018; Lun et al. 2017; Wang et al. 2018a], but their output models often lack resolution and sharp features necessary for high-quality 3D models.

To address these issues, in this paper we present a deep learning-based system to infer a complete man-made 3D shape from a single bitmap sketch. Given an expressive sketch of an object, our system infers a set of *parametric* surfaces that realize the drawing in 3D. The

component surfaces, parameterized by their control points, allow for easy editing in conventional shape editing software or conversion to a manifold mesh.

Most sketch-based modeling algorithms target natural shapes like humans and animals [Bessmeltsev et al. 2015; Entem et al. 2015; Igarashi et al. 1999], which are naturally smooth. To aid shape reconstruction, these systems promote smoothness of the reconstructed shape; representations like generalized cylinders are chosen to optimize in the space of smooth surfaces [Bessmeltsev et al. 2015; Entem et al. 2015]. This principle, however, does not apply to the focus of our work: man-made shapes. These objects, like planes or espresso machines, are only *piecewise* smooth and hence do not satisfy the assumptions of many sketch-based modeling systems.

In industrial design, man-made shapes are typically modeled using collections of smooth parametric patches, such as NURBS surfaces, with patch boundaries forming the sharp features. To learn such shapes effectively, we leverage this structure by using a special shape representation, a deformable parametric template [Jain et al. 1998]. This template is a manifold surface composed of patches, where each patch is parameterized by its control points; example patches include Bézier patches [Farin 2002] and Coons patches [Coons 1967] (Fig. 3(a)). This representation enables us to control the smoothness of each patch while allowing the model to introduce sharp edges between patches where necessary.

Compared to traditional representations, deformable parametric templates have numerous benefits for our task. They are intuitive to edit with conventional software, are resolution-independent, and can be meshed to arbitrary accuracy. Furthermore, since typically only boundary control points are needed, our surface representation has relatively few parameters to learn and store. Finally, this structure admits closed-form expressions for normals and other geometric features, which can be used to construct loss functions that improve reconstruction quality (§4.2).

The core of our system is a CNN-based architecture to infer the coordinates of control points of a deformable template, given a bitmap sketch. A naïve attempt to develop and train such network faces two major challenges: lack of data and the difficulty of detecting self-intersecting surfaces (Fig. 9(b,c)):

- A lack of data is the primary reason that sketch-based modeling has been slow to respond to developments in modern computer vision. Shape repositories are orders of magnitude smaller than image datasets, and supervised methods mapping from sketches to 3D models require a database of sketch-model pairs; to-date, there are no such large-scale repositories. Instead, we introduce a synthetic sketch augmentation pipeline that uses insights from the artistic literature to simulate possible variations observed in natural drawings (§3). Although our model is trained on synthetic sketches exclusively, it generalizes well to natural sketches (Fig. 8).
- To address the challenge of penalizing self-intersection, we bias the network to output non-self-intersecting surfaces. We train two networks to predict shape self-intersections given shape parameters. These networks (with frozen weights) act as additional loss terms in the optimization for sketch-based modeling to regularize our patches.

Contributions. We present a system for predicting parametric man-made 3D shapes from bitmap sketches. We validate with a gallery of results on both synthetic and natural sketches from various artists. Our key technical contributions include learning a different geometric representation, a novel sketch augmentation technique, and new loss terms with learned surface regularizers.

2 RELATED WORK

Our research leverages recent progress in deep learning to address long-standing problems in sketch-based modeling. To give a rough idea of the landscape of available methods, we briefly summarize related work in sketch-based modeling and deep learning.

2.1 Sketch-based 3D shape modeling

Reconstructing 3D geometry from sketches has a long history in the computer graphics literature. A complete survey of sketch-based modeling is beyond the scope of this paper; an interested reader may refer to the recent paper by Delanoy et al. [2018] or surveys by Ding and Liu [2016] and Olsen et al. [2009]. Here, we mention the work most relevant to our approach.

Many sketch-based 3D shape modeling systems are *incremental*, i.e., they allow users to model shapes by progressively adding new strokes, updating the 3D shape after each action. Such systems may be designed as *single-view* interfaces, where the user is often required to manually annotate each stroke [Chen et al. 2013; Cherlin et al. 2005; Gingold et al. 2009; Shtof et al. 2013], or they may allow strokes to be added to multiple views [Igarashi et al. 1999; Nealen et al. 2007; Tai et al. 2004]. These systems can cope with considerable geometric complexity, but their dependence on the ordering of the strokes forces artists to deviate from standard approaches to sketching. In contrast, we aim to interpret complete sketches, eliminating training for artists to use our system and enabling 3D reconstruction of legacy sketches. Xu et al. [2014] present a single-view 3D curve network reconstruction system for man-made shapes that can produce impressive sharp results. Yet, they process specialized *design* sketches, consisting of cross-sections, output only a curve network without the surface, and rely on user annotations. Our system produces complete 3D shapes from natural sketches with no extra annotation.

A variety of systems interpret a complete 2D sketch with no extra information. This species of input is extremely ambiguous thanks to hidden surfaces and noisy sketch curves, and hence reconstruction algorithms rely on strong 3D shape priors. These priors are typically manually created by experts. For example, priors for humanoid characters, animals, or natural shapes promote smooth, round, and symmetrical shapes [Bessmeltsev et al. 2015; Entem et al. 2015; Igarashi et al. 1999], while garments are typically regularized to be (piecewise-)developable [Jung et al. 2015; Li et al. 2017, 2018; Robson et al. 2011; Turquin et al. 2004; Zhu et al. 2013], and man-made shapes are often approximated as combinations of geometric primitives [Shao et al. 2016] or as unions of nearly-flat faces [Yang et al. 2013]. Our work focuses on man-made shapes, which have characteristic sharp edges and are only piecewise smooth rather than developable. We use a deformable patch template to promote shapes with this structure (§4.1). Moreover, introducing specific

expert-designed priors can be challenging: Man-made shapes are varied, diverse, and complex (Fig. 1,7,8). Instead, we *automatically* learn a separate, perhaps stronger, shape prior for each category of shapes from data. This stronger category-specific prior allows us to process ambiguous and complex sketches.

The vast majority of sketch-based modeling interfaces process vector input, which consists of a set of clean curves [Bessmeltsev et al. 2015, 2016; Entem et al. 2015; Jung et al. 2015; Li et al. 2017, 2018; Xu et al. 2014]. This approach is acceptable for tablet-based input, but it again may force the users to deviate from their preferred drawing media. Paper-and-pencil sketches still remain one of the most preferred means of capturing a shape. While those can be vectorized and cleaned up by modern methods [Bessmeltsev and Solomon 2019; Simo-Serra et al. 2018], preprocessing can introduce unnecessary distortions and errors into the drawing, leading to suboptimal reconstruction. In contrast, our system processes *bitmap* sketches, scanned or digital.

2.2 Deep learning for shape reconstruction

Learning to reconstruct 3D geometry from various input modalities recently has enjoyed significant research interest. Typical forms of input are images [Choy et al. 2016; Delanoy et al. 2018; Gao et al. 2019; Hane et al. 2018; Wang et al. 2018a; Wu et al. 2017; Yan et al. 2016] and point clouds [Groueix et al. 2018; Park et al. 2019; Williams et al. 2018]. When designing network for this task, two important questions affect the architecture: the loss function and the geometric representation.

Loss Functions. One promising and popular direction employs a differentiable renderer and measures 2D image loss between a rendering of the inferred 3D model and the input image, often called 2D-3D consistency or silhouette loss [Kato et al. 2018; Rezende et al. 2016; Tulsiani et al. 2018, 2017; Wu et al. 2017, 2016a; Yan et al. 2016]. A notable example is the work by Wu et al. [2017], which learns a mapping from a photograph to a three-piece output of normal map, depth map, and silhouette, as well as the mapping from this output to a voxelization. They use a differentiable renderer and measure inconsistencies in 2D. 2D losses are powerful in typical computer vision environments. Hand-drawn sketches, however, cannot be interpreted as perfect projections of 3D objects: They are imprecise and often inconsistent [Bessmeltsev et al. 2016]. Another approach uses 3D loss functions, measuring discrepancies between the predicted and target 3D shapes directly, often via Chamfer or a regularized Wasserstein distance [Gao et al. 2019; Groueix et al. 2018; Liu et al. 2010; Mandikal et al. 2018; Park et al. 2019; Williams et al. 2018], or—in the case of highly-structured representations such as voxel grids—sometimes cross-entropy [Hane et al. 2018]. We build on this work, adapting the Chamfer distance to our novel geometric representation and extending the loss function with new regularizers (§4.2).

Shape representation. As noted by Park et al. [2019], geometric representations in deep learning broadly can be divided into three classes: voxel-based representations, point-based representations, and mesh-based representations.

The most popular approach is to use voxels, directly reusing successful methods for 2D images [Choy et al. 2016; Delanoy et al. 2018; Tulsiani et al. 2018; Wang et al. 2018a,b; Wu et al. 2017, 2018; Yan et al. 2016; Zhang et al. 2018; Zhirong Wu et al. 2015]. The main limitation of voxel-based methods is low resolution due to memory limitations. Octree-based approaches mitigate this problem [Hane et al. 2018; Wang et al. 2017], learning shapes at up to 512^3 resolution, but even this density is insufficient to produce visually convincing surfaces. Furthermore, voxelized approaches cannot directly represent sharp features, which are key for man-made shapes.

Point-based approaches represent 3D geometry as a point cloud [Fan et al. 2017; Lun et al. 2017; Mandikal et al. 2018; Tatarchenko et al. 2015; Yang et al. 2018], sidestepping the memory issues. Those representations, however, do not capture connectivity. Hence, they cannot guarantee production of manifold surfaces.

Some recent methods explore the possibility of reconstructing mesh-based representations [Bagautdinov et al. 2018; Baqué et al. 2018; Kanazawa et al. 2018; Litany et al. 2017; Wang et al. 2019], representing shapes using deformable meshes. We take inspiration from this approach to reconstruct a surface by deforming a template, but our deformable parametric template representation allows us to more easily enforce piecewise smoothness and test for self-intersections (§4.2). These tasks are difficult to perform on meshes in a differentiable manner. Other mesh-based methods either use a precomputed parameterization to a domain on which it is straightforward to apply CNN-based architectures [Haim et al. 2018; Maron et al. 2017; Sinha et al. 2016] or learn a parameterization directly [Ben-Hamu et al. 2018; Groueix et al. 2018]. Even though these methods are not specifically designed for sketch-based modeling, for completeness, we compare our results to one of the more popular methods, AtlasNet [Groueix et al. 2018] (Fig. 13).

Finally, a few works explore less common representations, such as signed distance functions [Mescheder et al. 2018], implicit fields [Chen and Zhang 2018], implicit surfaces [Genova et al. 2019], shape programs [Tian et al. 2019], splines [Gao et al. 2019], volumetric primitives [Tulsiani et al. 2016; Zou et al. 2017], and elements of a learned latent space [Achlioptas et al. 2017; Wu et al. 2016b]. These papers demonstrate impressive reconstruction results, but either do not aim to produce an expressive complete 3D model [Gao et al. 2019; Tian et al. 2019; Tulsiani et al. 2016; Zou et al. 2017] or are not tuned to the problem of sketch reconstruction [Achlioptas et al. 2017; Chen and Zhang 2018; Genova et al. 2019; Mescheder et al. 2018; Wu et al. 2016b].

Very few deep learning algorithms address sketch-based 3D geometry reconstruction, with the notable exceptions of [Delanoy et al. 2018; Lun et al. 2017; Wang et al. 2018a]. Lun et al. [2017] use a CNN-based encoder-decoder architecture to predict multi-view depth and normal maps, later converted to point clouds. Wang et al. [2018a] successfully learn from separate unlabeled databases of sketches and 3D models with no correspondence between them. They train two networks: The first network is a GAN with an autoencoder-based discriminator aimed to embed both natural sketches and renders into a latent space with matching distributions. The second network is a more traditional CNN mapping the latent vector into a voxelization, trained on renders only. Another inspiration for our research is the work of Delanoy et al. [2018], which reconstructs a

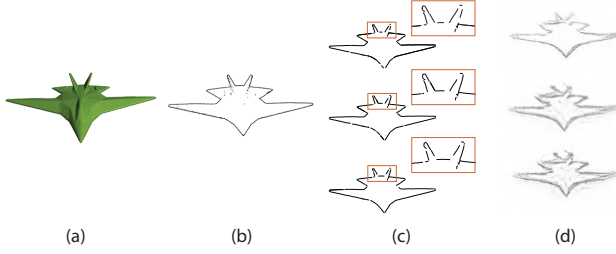


Fig. 2. Our data generation and augmentation pipeline. Starting with a 3D model (a), we use Autodesk Maya to generate its contours (b), which we vectorize using the method of Bessmeltsev and Solomon [2019] and stochastically modify (c). We then use the pencil drawing generation model of Simo-Serra et al. [2018] to generate the final image (d).

3D object, represented as voxelization, given sketches drawn from multiple views. We compare our results to results from these papers in Fig. 11. Because we target man-made shapes, we use a different shape representation—a deformable parametric template—which allows us to better capture the piecewise nature of the objects.

3 DATA PREPARATION

Since large-scale databases of hand-drawn sketches accompanied by 3D data are unavailable, we instead propose a method for generating synthetic training data from 3D models. Our system allows us to generate sketch-like images that capture a model from several views and contain the typical ambiguities and inaccuracies we expect to see in human-drawn sketches.

Our first step is to generate 2D contours from the 3D model, which an artist would capture in a sketch. Guided by the study by Cole et al. [2012], we render occluding contours and sharp edges using the Arnold Toon Shader in Autodesk Maya. We render each model from a fixed number of distinct camera views.

Although the contour images capture the main features of the 3D model, they lack some of the ambiguities present in natural sketches. We would like to augment our contour images with features such as broken lines to replicate the feeling of a rough hand-drawn sketch [Liu et al. 2018]. To this end, we first vectorize the contour images using the method of Bessmeltsev and Solomon [2019]. Then, for each vectorized image, we augment the set of contours. With a probability of 0.3, we split a random contour into two, introducing a gap at a uniformly random position. We do this no more than 10 times for a single image. Additionally, for each curve, we truncate it at its endpoints with probability of 0.2. Finally, we remove curves that are below a threshold in length.

In our final step, we introduce a realistic sketch-like texture to our contours while also introducing additional noise and ambiguity. For each augmented vectorized contour image, we rasterize it using several different stroke widths. We then pass the rasterized images through the pencil drawing generation model of Simo-Serra et al. [2018]. We illustrate our entire data generation and augmentation pipeline in Figure 2.

In the end, for each 3D model, we are able to obtain a series of realistic but synthetically-generated sketch images. In our experiments, we train on models with corresponding sketches from the

airplane, bathtub, guitar, and knife categories of the ShapeNet Core (v2) dataset [Chang et al. 2015]. We choose these categories because they largely contain models with similar consistent structure, making them well-suited for our representation, which we describe below. Prior to processing, we convert the ShapeNet models to watertight meshes using the method of Huang et al. [2018].

4 ALGORITHM

Equipped with a large dataset of sketch-like images and corresponding 3D shapes for training, we can engineer a pipeline that takes as input a raster sketch image and outputs a predicted 3D surface. We describe the geometric representation of the output surfaces (§4.1), define the loss terms that we optimize (§4.2), and specify the deep CNN architecture and training procedure (§4.3).

4.1 Representation

4.1.1 Patch Primitives. We would like to express 3D surfaces with a representation that is both compact and expressive. To capture the details of man-made shapes, our representation must be capable of containing smooth regions as well as sharp creases and corners. Given these requirements, we represent our surfaces as collections of parametric primitives, where each primitive is a Coons patch [Coons 1967].

A *Coons patch* is a parametric surface patch in three dimensions that is fully specified by four boundary curves sharing endpoints. We chose each boundary curve to be a *cubic Bézier curve*, $c(y)$, specified by four control vertices p_1, \dots, p_4 , two of which, p_1 and p_4 , are connected to adjacent vertices. Thus, a Coons patch is fully parameterized by 12 control vertices.

A single Bézier curve $c : [0, 1] \rightarrow \mathbb{R}^3$ is defined as

$$c(y) = p_1(1 - y)^3 + 3p_2y(1 - y)^2 + 3p_3y^2(1 - y) + p_4y^3, \quad (1)$$

and a Coons patch $P : [0, 1] \times [0, 1] \rightarrow \mathbb{R}^3$ is defined as

$$P(s, t) = (1 - t)c_1(s) + tc_3(1 - s) + sc_2(t) + (1 - s)c_4(1 - t) - (c_1(0)(1 - s)(1 - t) + c_1(1)s(1 - t) + c_3(1)(1 - s)t + c_3(0)st). \quad (2)$$

4.1.2 Templates. We introduce templates to specify the connectivity of a collection of Coons patches. A single template consists of the minimal number of control points necessary to the Coons patches, where some patches are adjacent to others, sharing boundary curves. For instance, we can define a template with cube topology consisting of six patches with 12 shared curves and 32 control points.

A template provides both a hard topological constraint for our surfaces as well as an initialization of their geometry (see §4.2.4). Thus, we define a distinct template for each category of shapes. In particular, we show our templates for the airplane, bathtub, guitar, and knife categories, consisting of 38, 14, and 22, respectively, in Figure 3. These templates are simple to construct, capturing only coarse geometric features and the approximate scale of their corresponding categories. However, they are crucial in ensuring that our predicted patches have consistent topology—an approach without templates would result in unstructured patch collections, with patches that do not align at boundaries or form a watertight surface.

Since each individual Coons patch is smooth and manifold whereas boundaries between adjacent patches are able to capture creases

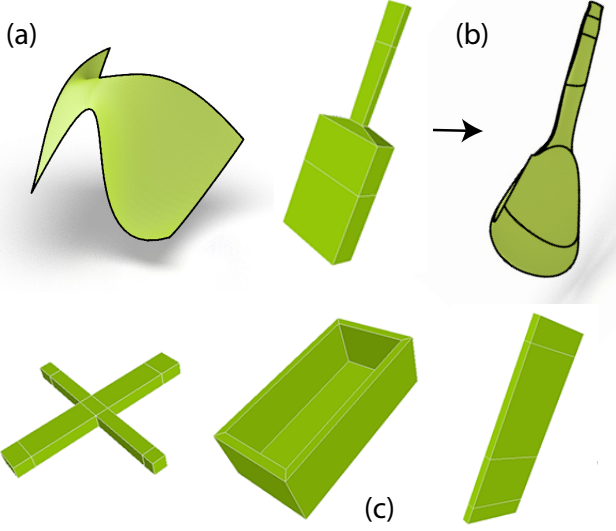


Fig. 3. Our geometry representation is composed of Coons patches (a) that are organized into a deformable template (b). We have designed a separate template per category of shapes: guitars (b), planes, bathtubs, and knives (c).

and corners, our choice of patch parameterization together with the templates yield a representation that is well-suited for our task.

4.2 Loss

In our training procedure, we would like to fit a collection of Coons patches $\{P_i\}$ to a target mesh M by optimizing a differentiable loss function. Below, we describe each term of our loss—a main reconstruction loss analogous to Chamfer distance (§4.2.1), a normal alignment loss (§4.2.2), and two regularizing losses to inhibit self-intersections (§4.2.3, §4.2.4).

4.2.1 Area-weighted Chamfer distance. Given two measurable shapes $A, B \subset \mathbb{R}^3$ and point sets X and Y sampled from A and B , respectively, the *directed Chamfer distance* between X and Y is

$$\text{Ch}_{\text{dir}}(X, Y) = \sum_{x \in X} \min_{y \in Y} d(x, y), \quad (3)$$

and the *symmetric Chamfer distance* is

$$\text{Ch}(X, Y) = \sum_{x \in X} \min_{y \in Y} d(x, y) + \sum_{x \in X} \min_{y \in Y} d(x, y), \quad (4)$$

where $d(x, y)$ is Euclidean distance between x and y .

Chamfer distance is differentiable and therefore a popular loss function in deep learning pipelines that optimize shapes (§2.2). It suffers from several disadvantages, however. In particular, the distribution under which X and Y are sampled from A and B has a significant impact on the Chamfer distance. In our setting, sampling uniformly from Coons patches is hard, and sampling uniformly from the parameter domain results in oversampling around regions of the patches with high curvature.

To address this sampling issue, following Smirnov et al. [2019], we first define the *variational Chamfer distance*, which follows naturally

from the original definition:

$$\text{Ch}_{\text{dir}}^{\text{var}}(A, B) = \int_A \inf_{y \in B} d(x, y) dx, \quad (5)$$

with symmetric variational Chamfer distance $\text{Ch}^{\text{var}}(A, B)$ defined analogously.

We leverage the fact that, while it is difficult to sample uniformly from our parametric patches, we are able to sample uniformly from their parameter domain (i.e., the unit square) in a straightforward fashion. Thus, we perform a change of variables:

$$\text{Ch}_{\text{dir}}^{\text{var}}(P, M) = \int_P \inf_{y \in M} d(x, y) dx \quad (6)$$

$$= \frac{1}{\text{Area}(P)} \int_P \inf_{y \in M} d(x, y) dS \quad (7)$$

$$= \frac{\mathbb{E}_{(u,v) \sim \mathcal{U}_{\square}} [\inf_{y \in M} d(P(u, v), y) |\det J|]}{\mathbb{E}_{(u,v) \sim \mathcal{U}_{\square}} [|\det J|]}, \quad (8)$$

where \mathcal{U}_{\square} is the uniform distribution on the parameter domain, dS is an area element on P , and J is the Jacobian of $P(u, v)$. In practice, we approximate this value via Monte Carlo sampling at each training iteration.

Since we can precompute points randomly sampled from the target mesh, we do not need to use this approach to compute $\text{Ch}_{\text{dir}}(M, P)$. Thus, our area-weighted Chamfer distance is

$$\mathcal{L}_{\text{Ch}}(\{P_i\}, M) = \frac{\sum_i \sum_{(u,v) \in \mathcal{U}_{\square}} \min_{x \in M} \|x - P_i(u, v)\|_2 |\det J(u, v)|}{\sum_{(u,v) \in \mathcal{U}_{\square}} |\det J(u, v)|} + \sum_{x \in M} \min_i \min_{y \in P_i} d(x, y), \quad (9)$$

where \mathcal{U}_{\square} is a set of points uniformly sampled from the unit square. We use symbolic evaluation software to compute the expression for $J(u, v)$ for a Coons patch in closed-form; this formula is computed once and compiled into our code.

4.2.2 Normal alignment. While the Chamfer distance loss term encourages our predicted patches to be close to the ground-truth mesh with respect to Euclidean distance, it contains no explicit notion of curvature or normal alignment. This results in surfaces that with curvature that differs significantly from the ground truth models (see §5.2). To address this, we add an additional normal alignment loss term.

This loss term is computed analogously to $\text{Ch}_{\text{dir}}(\{P_i\}, M)$, except that instead of Euclidean distance, we compute normal distance, defined as

$$d_N(x, y) = 1 - \langle n_x, n_y \rangle^2, \quad (10)$$

where n_x is the normal vector at point x . For each point y sampled from our predicted surface, we compare n_y to n_x , where $x \in M$ is closest to y under Euclidean distance. We precompute the normal vectors for all points sampled from our target meshes, and we again use symbolic differentiation to compute the expression for the normal vector of a Coons patch at $P(u, v)$.

In analogy to the variational Chamber loss above, we have

$$\mathcal{L}_{\text{normal}}(\{P_i\}, M) = \frac{\sum_i \sum_{(u,v) \in U_{\square}} (1 - \langle n_{\text{NN}(P_i(u,v), M)}, n_{P_i(u,v)} \rangle)^2 |\det J(u,v)|}{\sum_{(u,v) \in U_{\square}} |\det J(u,v)|}, \quad (11)$$

where $\text{NN}(x, Y)$ is the point closest to x in Y under Euclidean distance.

4.2.3 Intersection regularization. Using only the two loss terms described above, the surfaces output by our method would be constrained in topology via the prescribed template, but they would not be guaranteed to be watertight. In particular, they may suffer from self-intersections, both due to a single patch intersecting itself as well as two distinct patches intersecting each other. We propose two additional loss terms that regularize our training procedure, acting as soft constraints to prevent such defects.

Traditional parametric surface intersection tests, such as the Volino–Thalmann test [Andersson et al. 2007], are unfortunately only necessary and not sufficient. Other tests, such as Point Test Method [Andersson et al. 1997], are inapplicable to Coons patches or they can only be carried out via a procedure that is computationally expensive and non-differentiable [Patrikalakis and Maekawa 2002]. As an alternative approach better aligned to deep learning applications, we train two auxiliary multilayer perceptrons (MLPs) to approximate whether a patch intersects itself or whether two patches intersect each other. The *Coons self-intersection MLP* is a binary classifier that approximates the function $f : \mathbb{R}^{36} \rightarrow [0, 1]$, where the control points that define a Coons patch map to 1 if the patch self-intersects and 0 otherwise. Similarly, the *Coons pairwise intersection MLP* approximates the function $g : \mathbb{R}^{72} \rightarrow \{0, 1\}$, where an intersecting pair of Coons patches—expressed using $36 \times 2 = 72$ coordinates—maps to 1.

We generate about 50,000 training samples to train each MLP, making sure that the two classes are equally represented (there is an equal number of intersecting and non-intersecting samples). Each sample is generated by picking 12 (or 24) uniformly random control points and determining whether the resulting Coons patch (or pair of patches) is intersecting by converting the patches into a triangle mesh and testing the intersection of the mesh. During training, we augment our data with random isometries. In particular, we randomly rotate, reflect, and permute the control points of each patch or pair of patches. Additionally, we normalize the input such that each patch or pair of patches lies in the unit cube.

Each MLP consists of three layers with 1,024 units each, one layer with 512 units, one layer with 256 units, one layer 128 units, and an output layer with a single unit. We use Dropout [Srivastava et al. 2014] with a keep probability of 0.85 and ReLU after each hidden layer. We train the networks using Adam [Kingma and Ba 2014] with a learning rate of 10^{-4} , optimizing the cross-entropy loss for binary classification.

We attain classification accuracy 86.12% for self-intersections and 87.94% for pairwise intersections. While our regression problem is in principle binary, the real-valued score predicted by the MLPs roughly corresponds to the “severity” of intersection. We demonstrate this phenomenon in Figure 4, where we linearly interpolate

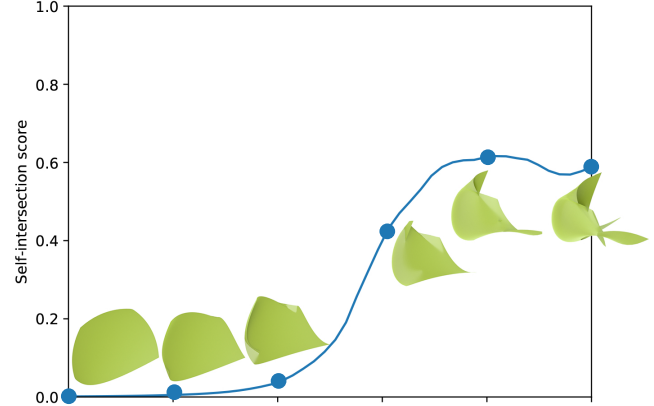


Fig. 4. Intersection scores predicted by the self-intersection MLP evaluated on 50 patches linearly interpolated between a flat patch and a patch with several self-intersections. The score increases as the patch becomes “more self-intersecting.” Six out of the 50 patches, including the initial and final patches, are displayed.

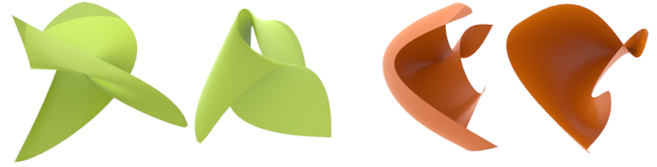


Fig. 5. Example patches misclassified by the self-intersection MLP. Two false positives (incorrectly predicted to be self-intersecting) are shown in green, and two false negatives are shown in orange.

between a flat patch and highly self-intersecting patch, plotting the scores for each patch in between. Note that the scores are nearly monotonically increasing. In Figure 5, we show some misclassified examples—typically the false negatives have only minor self-intersections, and the false positives are close to self-intersection.

We use these trained classifiers as fixed functions (with frozen weights) to define a self-intersection loss $\mathcal{L}_{\text{self-x}}(\{P_i\}) = \sum_i f(P_i)$ and pairwise intersection loss $\mathcal{L}_{\text{pair-x}}(\{P_i\}) = \sum_{i \neq j} g(P_i, P_j)$ in our main training procedure.

4.2.4 Template initialization. As described in §4.1.2, we employ a system of templates not only for constraining the Coons patch topology but also for providing an initialization for their geometry. Thus, following Smirnov et al. [2019], we add a template initialization loss term, which initializes the network output to the template patch parameters and decays exponentially as training progresses:

$$\mathcal{L}_{\text{template}}(\{P_i\}) = \sum_i \gamma^{(t/s)} \|P_i - T_i\|_2^2, \quad (12)$$

where $\gamma \in (0, 1)$ and $s > 0$ are decay parameters, t is the current training iteration, and T_i is the template for the i th Coons patch. In our experiments, we set $\gamma = 0.4$ and $s = 600$.

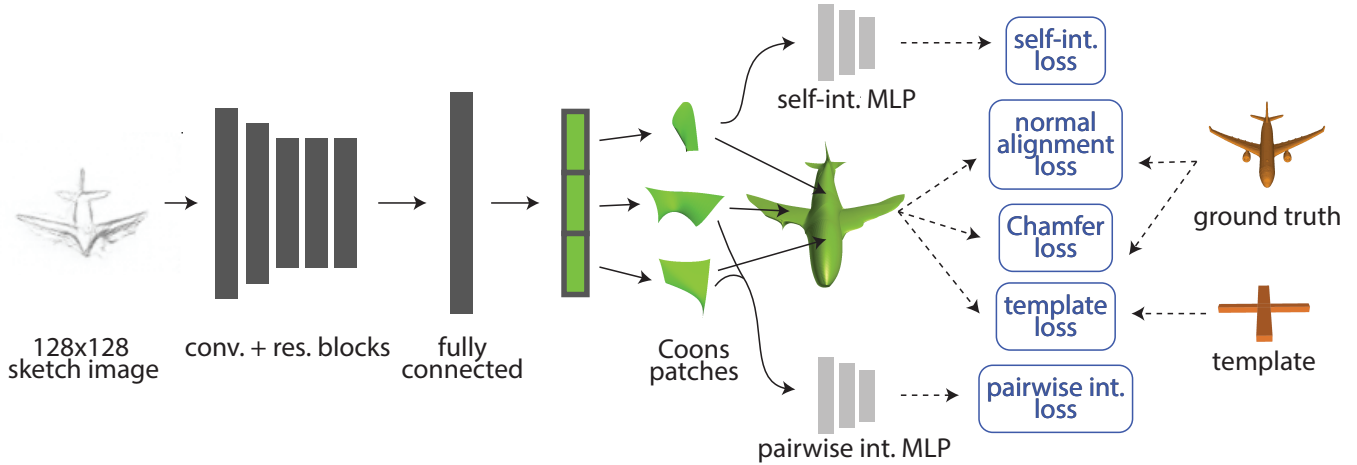


Fig. 6. An overview of our deep learning pipeline. We encode a sketch image with a series of convolutions and residual blocks. Following a fully connected layer, we get back a series of parameters defining a collection of Coons patches. We then compute five loss values based on the predicted patches and the ground truth 3D model as well as a template. We optimize the overall loss using backpropagation.

4.3 Deep learning pipeline

The final loss that we optimize is

$$\begin{aligned} \mathcal{L}(\{P_i\}, M) = & \alpha_{\text{Ch}} \mathcal{L}_{\text{Ch}}(\{P_i\}, M) \\ & + \alpha_{\text{normal}} \mathcal{L}_{\text{normal}}(\{P_i\}, M) \\ & + \alpha_{\text{template}} \mathcal{L}_{\text{template}}(\{P_i\}) \\ & + \alpha_{\text{self-x}} \mathcal{L}_{\text{self-x}}(\{P_i\}) \\ & + \alpha_{\text{pair-x}} \mathcal{L}_{\text{pair-x}}(\{P_i\}). \end{aligned} \quad (13)$$

To do so, we train a CNN, which takes as input a 128×128 raster image of a sketch. We use an encoder-style architecture, consisting of seven convolutional layers followed by seven residual blocks [He et al. 2016], two additional alternating convolutional layers and residual blocks, two fully-connected layers with 512 and 256 units, respectively, and a final fully-connected layer with size equal to the appropriate output dimension. We use the ELU nonlinearity [Clevert et al. 2015] after each layer except for the last; LayerNorm [Ba et al. 2016] after each convolutional and residual layer, except for the first; and dilated convolutions in the residual blocks [Yu and Koltun 2016]. We train each network on a single Tesla K80 GPU, using Adam [Krizhevsky et al. 2012] with learning rate 10^{-4} and batch size 16. At each iteration, we sample 5,000 points from the predicted and target shapes. Training the model takes approximately 12 hours, and a forward pass takes approximately 270 milliseconds. Our entire pipeline is illustrated in Figure 6.

5 EXPERIMENTAL RESULTS

We demonstrate the efficacy of our method with a series of experiments. First, we show 3D reconstruction results both on synthetic sketches from our dataset as well as natural human-drawn sketches. We also perform an ablation study, demonstrating the necessity of each component of our system. Finally, we compare our results to existing methods.

5.1 Results on Real and Synthetic Sketches

We evaluate our method on synthetic sketches from our test dataset for each object category in Figure 7. Our method is able to convey distinctive features and details of the sketches from various viewpoints in the 3D reconstructions.

We also test our method on real sketches drawn by four artists using pencil and paper as well as an iPad with an Apple Pencil. Each artist was shown a rendering of a sample 3D model (airplane and bathtub) rendered from each of our supported viewpoints and was told to sketch an object in the same category from one of the viewpoints. The artists were never shown the contours or synthetic sketches used in our training procedure.

The 3D results that we recover are similar to those on the synthetic sketches. This demonstrates that our dataset is reflective of the choices that humans make when sketching 3D objects.

5.2 Ablation Study

We perform an ablation study of our method. We demonstrate results on a human-drawn airplane sketch for a network trained without each of the loss terms, with a template using fewer patches, and with training data generated without several steps of our data generation procedure. The results are shown in Figure 9.

The ablation study demonstrates the contribution of each component of our system method to the final result. Training without each of the intersection loss results in predictions containing pairwise or self-intersections. Omitting the normal loss causes the 3D surface to suffer in smoothness. Using a simpler template with fewer patches (we show the full and simple templates in Figure 10) is at the expense of details captured in the 3D prediction, e.g. the tail of the airplane. Finally, removing the pencil sketch filter and/or the vector contour augmentation results in less realistic reconstructions.



Fig. 7. Results on synthetic sketches taken from our test datasets for bathtubs, guitars, and knives.

5.3 Comparisons

In Figure 11, we compare our method to the sketch-based 3D reconstruction methods of Lun et al. [2017] and Delanoy et al. [2018]. Our comparisons are generated using the species of input used to train these two methods, rather than attempting to re-train their models for our input. Moreover, both of these methods perform 3D reconstruction from *multiple* sketches, while we are able to produce similar results from a single sketch.

Although we train on a different dataset, the visual quality and fidelity of our predictions is comparable to the output of [Lun et al. 2017] and [Delanoy et al. 2018]. Moreover, our method offers some distinct advantages. In particular, we output a 3D representation that sparsely captures smooth and sharp features, independent of resolution. In contrast, Delanoy et al. [2018] produce a 64^3 voxel grid—a dense representation at a fixed resolution, which cannot be edited directly and offers no topological guarantees. In Figure 12, we show results of their system evaluated on contours from our dataset.

These inputs were not processed with the pencil sketch model, to more closely resemble the data used to train their system. We show their results (orange) on two inputs alongside our results (green). These results largely demonstrate that our task of reconstructing single-viewpoint sketches with a prior on class (airplane) rather than geometric structure (cylinders and cuboids) is misaligned with theirs: Since our training data is not well-approximated by CSG models, their method is unable to extract meaningful output.

Although the method of Lun et al. [2017] ultimately produces a mesh, it is only after a computationally expensive post-processing and fine-tuning procedure, since a forward pass through their network returns a labeled point cloud from which the mesh is extracted. Our method directly outputs the parameters for surface patches with no further optimization or post-processing. Additionally, the final mesh from their technique contains more components (triangles) than our output representation (patches), making it less useful for editing. Finally, their fine-tuning approach is fundamentally incompatible with the goal of parsing human-drawn sketches, since they

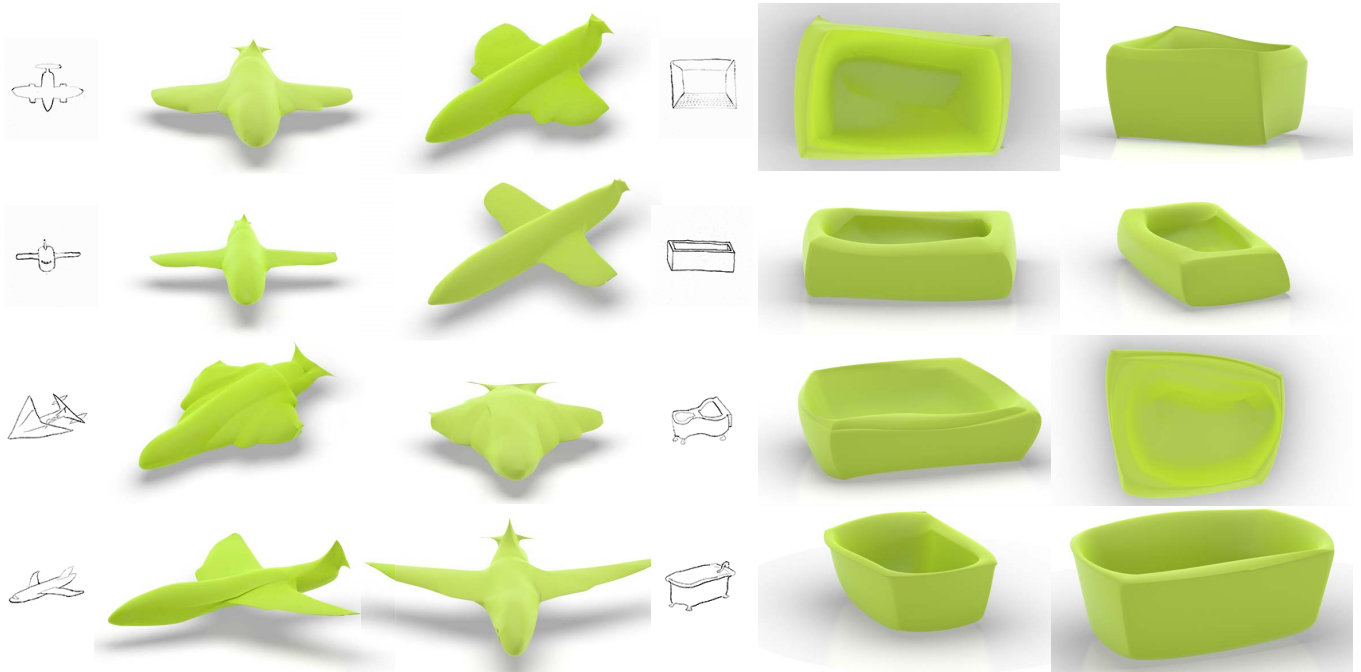


Fig. 8. Results on real human-drawn sketches. The top two rows are sketches are drawn on pencil and paper and scanned while the bottom two rows are drawn on iPad. Each artist was shown the sample sample 3D models rendered from several viewpoints but was not provided with sample sketches or given instructions on how to draw the sketches.

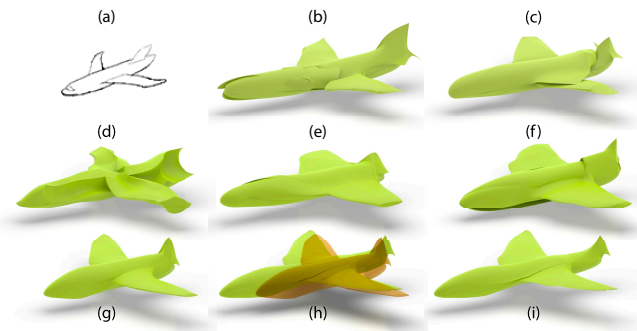


Fig. 9. For a human-drawn sketch (a), we perform an ablation study of our algorithm, training the network (b) without the self-intersection loss, (c) without pairwise intersection loss, (d) without normal loss, or using a simple template (e). We also study the effects of various data augmentation stages (§3) by training the network: (f) only on contour renders without any augmentation, (g) with the sketch filter, but no vector augmentation. In (h), we overlay (g, shown in brown) with the final result (i).

rely on propagating changes to the 3D mesh back to the raster image. The inherent ambiguity and noise of our input precludes this procedure.

In Figure 13, we compare our method to AtlasNet [Groueix et al. 2018]. Since AtlasNet does not operate on sketch-based input, we retrain our model with the renderings used for AtlasNet. While our 3D reconstructions capture the same amount of detail, they do not

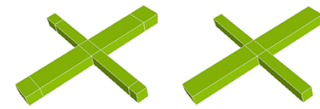


Fig. 10. The template used for our main airplane model (left) and the simple airplane template used for the ablation study (right). The simple airplane template contains fewer patches than the main template, and, consequently, yields less expressive results.

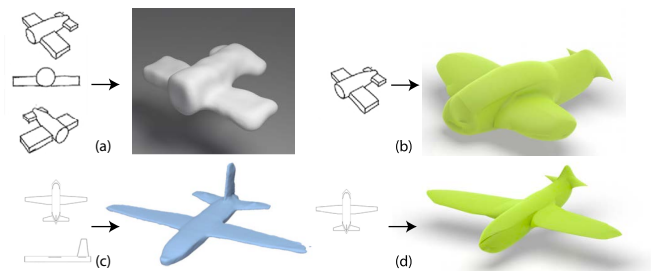


Fig. 11. Compared to the previous *multi-view* approaches, [Delaney et al. 2018] (a) and [Lun et al. 2017] (c), we (b and d) produce results of comparable quality with just a single sketch. Furthermore, unlike voxelization-based approaches [Delaney et al. 2018] or smooth mesh-based [Lun et al. 2017], our models don't depend on resolution and can represent sharp and smooth regions explicitly.



Fig. 12. Comparison to [Delaney et al. 2018] for single-view reconstruction on inputs from our dataset. Their predictions (graciously generated by the authors) are in orange, and ours are in green. This experiment demonstrates that their method does not generalize to arbitrary single-view sketches.



Fig. 13. 3D reconstructions using AtlasNet [Groueix et al. 2018] (b) and our method (c) given a single rendering as input (a). Compared to AtlasNet, we produce a result without topological defects (holes and overlaps). Additionally, each of our patch primitives is easily editable and has a low dimensional, interpretable parameterization.

suffer from the topological defects of AtlasNet’s representation. In particular, AtlasNet’s reconstruction contains many patch intersections as well as holes in the surface. Extracting a watertight mesh would require significant post-processing. Additionally, each patch in our representation is parameterized sparsely by control points on its boundary. This is in contrast to AtlasNet’s patches, which come from a learned latent space and must be sampled using a deep decoder network.

6 DISCUSSION AND CONCLUSION

Sketch-based modeling is a singularly challenging task representative of the difficulties that arise when coupling learning and graphics. A system for this task must infer clean features from rough curves, depth from 2D, and missing features from a single view. But the potential payoff is singular as well: As algorithms in this area reach higher and higher levels of practicality, sketch-based modeling holds potential to change how we design 3D shapes fundamentally.

While many difficult problems remain on the path toward this goal, our system represents a significant step toward practical 3D modeling from sketches. Our use of a sparse patch-based representation is closer to what is used in artistic and engineering practice, and we accompany this representation with new geometric and learned regularizers that greatly improve the reconstruction process. Unlike meshes or voxel occupancy functions, this representation can easily be edited and tuned after 3D reconstruction, and it captures a trade-off between smoothness and sharp edges reasonable for man-made shapes. Furthermore, our synthetic sketch data generation pipeline fills a gap in data sets needed to train modern machine learning systems for this task.

Our work suggests several avenues for future research. Currently our technique uses pre-trained networks to generate sketch training data and to penalize patch intersection; inspired by recent generative adversarial networks (GAN), we could couple together training of these different pieces to alleviate dependence on matched sketch–3D model pairs. We also could explore coupling with other representations, leveraging the rich literature in computer-aided

geometric design (CAGD) to identify other structures amenable to learning with relatively few parameters. Of particular interest are multiresolution representations (e.g., subdivision surfaces), which might enable the system to learn both high-level smooth structure as well as geometric details like filigree independently. It also may be beneficial to incorporate additional modalities such as photographs to further regularize our learned output.

Other extensions of our work might be oriented on the end user. Capturing and learning from the sequence of strokes might be fruitful for disambiguating depth information in 3D reconstruction. Furthermore, we should close the loop between learning system and artist, allowing the artist to edit the 3D model or to edit the sketch and have the changes propagate to the other side.

Perhaps the most important challenge remaining from our work—and others, such as [Kanazawa et al. 2018; Smirnov et al. 2019; Wang et al. 2019]—involves inference of the *topology* of a shape. Currently we rely on a per-class template to determine connectivity of patch vertices. Although this limitation is reasonable for the classes of shapes we consider—and likely for *parts* of shapes, as explored in [Mo et al. 2019]—reconstruction of a sketch of a generic full shape will require algorithms that automatically add and connect patches in a flexible and adaptive fashion. The technical issue here is that introduction of patches or couplings between control points is fundamentally a discrete decision, which can be incompatible with conventional deep learning methods.

Even without the improvements above, our system remains an effective means of 3D shape recovery from sketches. It can be used as a means of extracting an initial 3D model that can be tuned by an artist or engineer. Moreover, our architecture and loss functions can be incorporated as building blocks into larger pipelines connecting artistic imagery to the 3D world.

7 ACKNOWLEDGEMENT

We acknowledge the generous support of Army Research Office grant W911NF-12-R-0011, of National Science Foundation grant IIS-1838071, from an Amazon Research Award, from the MIT-IBM Watson AI Laboratory, from the Toyota-CSAIL Joint Research Center, from the Skoltech-MIT Next Generation Program, and of a gift from Adobe Systems. This work was also supported by the National Science Foundation Graduate Research Fellowship under Grant No. 1122374. We acknowledge the support of the Natural Sciences and Engineering Research Council of Canada (NSERC) grant RGPIN-2019-05097 (“Creating Virtual Shapes via Intuitive Input”) and from the Fonds de recherche du Québec - Nature et technologies (FRQNT) grant 2020-NC-270087.

REFERENCES

- Panos Achlioptas, Olga Diamanti, Ioannis Mitliagkas, and Leonidas J Guibas. 2017. Learning Representations and Generative Models For 3D Point Clouds. *arXiv preprint arXiv:1707.02392* (2017).
- L.E. Andersson, T. J. Peters, and N. F. Stewart. 1997. Self-Intersection of Composite Curves and Surfaces. *Computer Aided Geometric Design* 15 (1997), 507–527.
- L. Andersson, N. Stewart, and M. Zidani. 2007. Error Analysis for Operations in Solid Modeling in the Presence of Uncertainty. *SIAM Journal on Scientific Computing* 29, 2 (2007), 811–826. <https://doi.org/10.1137/040604303> arXiv:<https://doi.org/10.1137/040604303>
- Jimmy Lei Ba, Jamie Ryan Kiros, and Geoffrey E Hinton. 2016. Layer normalization. *arXiv preprint arXiv:1607.06450* (2016).

- Timur Bagautdinov, Chenglei Wu, Jason Saragih, Pascal Fua, and Yaser Sheikh. 2018. Modeling Facial Geometry Using Compositional VAEs. In *The IEEE Conference on Computer Vision and Pattern Recognition (CVPR)*.
- Pierre Baqué, Edoardo Remelli, Francois Fleuret, and Pascal Fua. 2018. Geodesic Convolitional Shape Optimization. (02 2018).
- Heli Ben-Hamu, Haggai Maron, Itay Kezurer, Gal Avineri, and Yaron Lipman. 2018. Multi-chart Generative Surface Modeling. *ACM Trans. Graph.* 37, 6, Article 215 (Dec. 2018), 15 pages. <https://doi.org/10.1145/3272127.3275052>
- Mikhail Bessmeltsev, Will Chang, Nicholas Vining, Alla Sheffer, and Karan Singh. 2015. Modeling Character Canvases from Cartoon Drawings. *ACM Trans. Graph.* 34, 5, Article 162 (Nov. 2015), 16 pages. <https://doi.org/10.1145/2801134>
- Mikhail Bessmeltsev and Justin Solomon. 2019. Vectorizing Line Drawings via Polyvector Fields. *ACM Transactions on Graphics* 38, 1 (2019).
- Mikhail Bessmeltsev, Nicholas Vining, and Alla Sheffer. 2016. Gesture3D: Posing 3D Characters via Gesture Drawings. *ACM Transactions on Graphics* 35, 6 (2016), 165:1–165:13. <https://doi.org/10.1145/2980179.2980240>
- Angel X. Chang, Thomas Funkhouser, Leonidas Guibas, Pat Hanrahan, Qixing Huang, Zimo Li, Silvio Savarese, Manolis Savva, Shuran Song, Hao Su, Jianxiong Xiao, Li Yi, and Fisher Yu. 2015. *ShapeNet: An Information-Rich 3D Model Repository*. Technical Report arXiv:1512.03012 [cs.GR]. Stanford University – Princeton University – Toyota Technological Institute at Chicago.
- Tao Chen, Zhe Zhu, Ariel Shamir, Shi-Min Hu, and Daniel Cohen-Or. 2013. 3-Sweep. *ACM Transactions on Graphics* 32, 6 (2013), 1–10. <https://doi.org/10.1145/2508363.2508378>
- Zhiqin Chen and Hao Zhang. 2018. Learning Implicit Fields for Generative Shape Modeling. (2018). arXiv:1812.02822 <http://arxiv.org/abs/1812.02822>
- Joseph Jacob Cherlin, Faramarz Samavati, Mario Costa Sousa, and Joaquim A. Jorge. 2005. Sketch-based modeling with few strokes. *Proceedings of the 21st spring conference on Computer graphics - SCCG '05* 1, 212 (2005), 137. <https://doi.org/10.1145/1090122.1090145>
- Christopher B. Choy, Danfei Xu, Jun Young Gwak, Kevin Chen, and Silvio Savarese. 2016. 3D-R2N2: A unified approach for single and multi-view 3D object reconstruction. *Lecture Notes in Computer Science (including subseries Lecture Notes in Artificial Intelligence and Lecture Notes in Bioinformatics)* 9912 LNCS (2016), 628–644. https://doi.org/10.1007/978-3-319-46484-8_38 arXiv:arXiv:1604.00449v1
- Djork-Arné Clevert, Thomas Unterthiner, and Sepp Hochreiter. 2015. Fast and accurate deep network learning by exponential linear units (elus). *arXiv preprint arXiv:1511.07289* (2015).
- Forrester Cole, Aleksey Golovinskiy, Alex Limpaecher, Heather Stoddart Barros, Adam Finkelstein, Thomas Funkhouser, and Szymon Rusinkiewicz. 2012. Where do people draw lines? *Commun. ACM* 55, 1 (2012), 107. <https://doi.org/10.1145/2063176.2063202>
- S. A. Coons. 1967. *Surfaces for Computer-Aided Design of Space Forms*. Technical Report. Cambridge, MA, USA.
- Johanna Delanoy, Mathieu Aubry, Phillip Isola, Alexei A. Efros, and Adrien Bousseau. 2018. 3D Sketching using Multi-View Deep Volumetric Prediction. *3D* (2018). <https://doi.org/10.1145/nnnnnnnn.nnnnnnnn> arXiv:arXiv:1603.09436
- Chao Ding and Ligang Liu. 2016. A Survey of Sketch Based Modeling Systems. *Front. Comput. Sci.* 10, 6 (Dec. 2016), 985–999. <https://doi.org/10.1007/s11704-016-5422-9>
- Even Entem, Loic Barthe, Marie-Paule Cani, Frederic Cordier, and Michiel van de Panne. 2015. Modeling 3D Animals from a Side-view Sketch. *Comput. Graph.* 46, C (Feb. 2015), 221–230. <https://doi.org/10.1016/j.cag.2014.09.037>
- Haoqiang Fan, Hao Su, and Leonidas Guibas. 2017. DeepPointSet: A Point Set Generation Network for 3D Object Reconstruction from a Single Image. In *CVPR*.
- Gerald Farin. 2002. *Curves and Surfaces for CAGD: A Practical Guide* (5th ed.). Morgan Kaufmann Publishers Inc., San Francisco, CA, USA.
- Jun Gao, Chengcheng Tang, Vignesh Ganapathi-Subramanian, Jiahui Huang, Hao Su, and Leonidas J. Guibas. 2019. DeepSpline: Data-Driven Reconstruction of Parametric Curves and Surfaces. (2019), 1–13. arXiv:1901.03781 <http://arxiv.org/abs/1901.03781>
- Kyle Genova, Forrester Cole, Daniel Vlasic, Aaron Sarna, William T. Freeman, and Thomas A. Funkhouser. 2019. Learning Shape Templates with Structured Implicit Functions. *CoRR* abs/1904.06447 (2019). arXiv:1904.06447 <http://arxiv.org/abs/1904.06447>
- Yotam Gingold, Takeo Igarashi, and Denis Zorin. 2009. Structured annotations for 2D-to-3D modeling. *ACM Transactions on Graphics* 28, 5 (2009), 1. <https://doi.org/10.1145/1618452.1618494>
- Thibault Groueix, Matthew Fisher, Vladimir G. Kim, Bryan C. Russell, and Mathieu Aubry. 2018. AtlasNet: A Papier-Mache Approach to Learning 3D Surface Generation. *Proceedings of the IEEE Computer Society Conference on Computer Vision and Pattern Recognition* (2018), 216–224. <https://doi.org/10.1109/CVPR.2018.00030> arXiv:arXiv:1802.05384v3
- Niv Haim, Nimrod Segol, Heli Ben Hamu, Haggai Maron, and Yaron Lipman. 2018. Surface Networks via General Covers. *CoRR* abs/1812.10705 (2018). arXiv:1812.10705 <http://arxiv.org/abs/1812.10705>
- Christian Hane, Shubham Tulsiani, and Jitendra Malik. 2018. Hierarchical surface prediction for 3D object reconstruction. *Proceedings - 2017 International Conference on 3D Vision, 3DV 2017* (2018), 412–420. <https://doi.org/10.1109/3DV.2017.00054> arXiv:arXiv:1704.00710v2
- Kaiming He, Xiangyu Zhang, Shaoqing Ren, and Jian Sun. 2016. Deep residual learning for image recognition. In *Proceedings of the IEEE conference on computer vision and pattern recognition*. 770–778.
- Jingwei Huang, Hao Su, and Leonidas Guibas. 2018. Robust Watertight Manifold Surface Generation Method for ShapeNet Models. *arXiv preprint arXiv:1802.01698* (2018).
- Takeo Igarashi, Satoshi Matsuoka, and Hidehiko Tanaka. 1999. Teddy: A Sketching Interface for 3D Freeform Design. In *Proceedings of the 26th Annual Conference on Computer Graphics and Interactive Techniques (SIGGRAPH '99)*. ACM Press/Addison-Wesley Publishing Co., New York, NY, USA, 409–416. <https://doi.org/10.1145/311535.311602>
- Anil K. Jain, Yu Zhong, and Marie-Pierre Dubuisson-Jolly. 1998. Deformable Template Models: A Review. *Signal Process.* 71, 2 (Dec. 1998), 109–129. [https://doi.org/10.1016/S0165-1684\(98\)00139-X](https://doi.org/10.1016/S0165-1684(98)00139-X)
- A Jung, S Hahmann, D Rohmer, A Begault, L Boissieux, and M P Cani. 2015. Sketching Folds: Developable Surfaces from Non-Planar Silhouettes. *ACM Transactions on Graphics* 34, 5 (2015), 12. <https://doi.org/10.1145/2749458>
- Angjoo Kanazawa, Shubham Tulsiani, Alexei A. Efros, and Jitendra Malik. 2018. Learning Category-Specific Mesh Reconstruction from Image Collections. In *ECCV*. 1–21. arXiv:arXiv:1803.07549v2
- Hiroharu Kato, Yoshitaka Ushiku, and Tatsuya Harada. 2018. Neural 3D Mesh Renderer. In *The IEEE Conference on Computer Vision and Pattern Recognition (CVPR)*.
- Diederik P Kingma and Jimmy Ba. 2014. Adam: A method for stochastic optimization. *arXiv preprint arXiv:1412.6980* (2014).
- Alex Krizhevsky, Ilya Sutskever, and Geoffrey E Hinton. 2012. Imagenet classification with deep convolutional neural networks. In *Advances in neural information processing systems*. 1097–1105.
- Changjian Li, Hao Pan, Xin Tong, Alla Sheffer, and Wenping Wang. 2017. BendSketch: Modeling Freeform Surfaces Through 2D Sketching. *ACM Trans. Graph.* 36, 4 (2017).
- Minchen Li, Alla Sheffer, Eitan Grinspun, and Nicholas Vining. 2018. Foldsketch: enriching garments with physically reproducible folds. *[ACM] Trans. Graph.* 37, 4 (2018), 133:1–133:13.
- Or Litany, Alex Bronstein, Michael Bronstein, and Ameesh Makadia. 2017. Deformable Shape Completion with Graph Convolutional Autoencoders. (12 2017).
- Chenxi Liu, Enrique Rosales, and Alla Sheffer. 2018. StrokeAggregator: Consolidating Raw Sketches into Artist-Intended Curve Drawings. *ACM Transaction on Graphics* 37, 4 (2018). <https://doi.org/10.1145/3197517.3201314>
- M. Liu, O. Tuzel, A. Veeraraghavan, and R. Chellappa. 2010. Fast directional chamfer matching. In *2010 IEEE Computer Society Conference on Computer Vision and Pattern Recognition*. 1696–1703. <https://doi.org/10.1109/CVPR.2010.5539837>
- Zhaoliang Lun, Mathieu Gadelha, Evangelos Kalogerakis, Subhransu Maji, and Rui Wang. 2017. 3D Shape Reconstruction from Sketches via Multi-view Convolutional Networks. (2017). <https://doi.org/10.1109/3dv.2017.00018> arXiv:1707.06375
- Priyanka Mandikal, K L Navaneet, Mayank Agarwal, and R. Venkatesh Babu. 2018. 3D-LMNet: Latent Embedding Matching for Accurate and Diverse 3D Point Cloud Reconstruction from a Single Image. (2018), 1–19. arXiv:1807.07796 <http://arxiv.org/abs/1807.07796>
- Haggai Maron, Meirav Galun, Noam Aigerman, Miri Trope, Nadav Dym, Ersin Yumer, Vladimir G. Kim, and Yaron Lipman. 2017. Convolutional Neural Networks on Surfaces via Seamless Toric Covers. *ACM Trans. Graph.* 36, 4, Article 71 (July 2017), 10 pages. <https://doi.org/10.1145/3072959.3073616>
- Lars Mescheder, Michael Oechsle, Michael Niemeyer, Sebastian Nowozin, and Andreas Geiger. 2018. Occupancy Networks: Learning 3D Reconstruction in Function Space. (2018). arXiv:1812.03828 <http://arxiv.org/abs/1812.03828>
- Kaichun Mo, Shilin Zhu, Angel Chang, Li Yi, Subarna Tripathi, Leonidas Guibas, and Hao Su. 2019. PartNet: A Large-scale Benchmark for Fine-grained and Hierarchical Part-level 3D Object Understanding. In *Proceedings of the IEEE Conference on Computer Vision and Pattern Recognition (CVPR)*.
- Andrew Nealen, Takeo Igarashi, Olga Sorkine, and Marc Alexa. 2007. FiberMesh: Designing Freeform Surfaces with 3D Curves. *ACM Trans. Graph.* 26, 3, Article 41 (July 2007). <https://doi.org/10.1145/1276377.1276429>
- Luke Olsen, Faramarz F. Samavati, Mario Costa Sousa, and Joaquim A. Jorge. 2009. Sketch-based modeling: A survey. *Computers & Graphics* 33, 1 (feb 2009), 85–103. <https://doi.org/10.1016/j.cag.2008.09.013>
- Jeong Joon Park, Peter Florence, Julian Straub, Richard Newcombe, and Steven Lovegrove. 2019. DeepSDF: Learning Continuous Signed Distance Functions for Shape Representation. (2019). arXiv:1901.05103 <http://arxiv.org/abs/1901.05103>
- Nicholas Patrikalakis and Takashi Maekawa. 2002. *Shape Interrogation for Computer Aided Design and Manufacturing*.
- Danilo Jimenez Rezende, S. M. Ali Eslami, Shakir Mohamed, Peter Battaglia, Max Jaderberg, and Nicolas Heess. 2016. Unsupervised Learning of 3D Structure from Images. *Nips* (2016). arXiv:1607.00662 <http://arxiv.org/abs/1607.00662>
- C. Robson, R. Maharik, A. Sheffer, and N. Carr. 2011. Context-Aware Garment Modeling from Sketches. *Computers and Graphics (Proc. SMI 2011)* (2011), 604–613.
- Tianjia Shao, Dongping Li, Yuliang Rong, Changxi Zheng, and Kun Zhou. 2016. Dynamic Furniture Modeling Through Assembly Instructions. *ACM Trans. Graph.* 35, 6, Article

- 172 (Nov. 2016), 15 pages. <https://doi.org/10.1145/2980179.2982416>
- A. Shtof, A. Agathos, Y. Gingold, A. Shamir, and D. Cohen-Or. 2013. Geosemantic Snapping for Sketch-Based Modeling. *Computer Graphics Forum* 32, 2, pt. 2 (may 2013), 245–253. <https://doi.org/10.1111/cgf.12044>
- Edgar Simo-Serra, Satoshi Iizuka, and Hiroshi Ishikawa. 2018. Mastering Sketching: Adversarial Augmentation for Structured Prediction. *Transactions on Graphics (Presented at SIGGRAPH)* 37, 1 (2018).
- Ayan Sinha, Jing Bai, and Karthik Ramani. 2016. Deep Learning 3D Shape Surfaces Using Geometry Images. In *ECCV*.
- Dmitriy Smirnov, Matthew Fisher, Vladimir G. Kim, Richard Zhang, and Justin Solomon. 2019. Deep Parametric Shape Predictions using Distance Fields. (April 2019). <https://arxiv.org/abs/1904.08921>
- Nitish Srivastava, Geoffrey Hinton, Alex Krizhevsky, Ilya Sutskever, and Ruslan Salakhutdinov. 2014. Dropout: A Simple Way to Prevent Neural Networks from Overfitting. *J. Mach. Learn. Res.* 15, 1 (Jan. 2014), 1929–1958. <http://dl.acm.org/citation.cfm?id=2627435.2670313>
- Chiew-Lan Tai, Hongxin Zhang, and Jacky Chun-Kin Fong. 2004. Prototype Modeling from Sketched Silhouettes based on Convolution Surfaces. *Computer Graphics Forum* (2004). <https://doi.org/10.1111/j.1467-8659.2004.00006.x>
- Maxim Tatarchenko, Alexey Dosovitskiy, and Thomas Brox. 2015. Multi-view 3D Models from Single Images with a Convolutional Network. (2015). <https://doi.org/10.1613/jair.301> arXiv:1511.06702
- Yonglong Tian, Andrew Luo, Xingyuan Sun, Kevin Ellis, William T. Freeman, Joshua B. Tenenbaum, and Jiajun Wu. 2019. Learning to Infer and Execute 3D Shape Programs. In *International Conference on Learning Representations*.
- Shubham Tulsiani, Alexei A. Efros, and Jitendra Malik. 2018. Multi-view Consistency as Supervisory Signal for Learning Shape and Pose Prediction. (2018). arXiv:1801.03910 <http://arxiv.org/abs/1801.03910>
- Shubham Tulsiani, Hao Su, Leonidas Guibas, Alexei A. Efros, and Jitendra Malik. 2016. Learning Shape Abstractions by Assembling Volumetric Primitives. (2016). <https://doi.org/10.1109/CVPR.2017.160> arXiv:1612.00404
- Shubham Tulsiani, Tinghui Zhou, Alexei A. Efros, and Jitendra Malik. 2017. Multi-view Supervision for Single-view Reconstruction via Differentiable Ray Consistency. (2017). <https://doi.org/10.1109/CVPR.2017.30> arXiv:1704.06254
- Emmanuel Turquin, Marie-Paule Cani, and John F. Hughes. 2004. Sketching Garments for Virtual Characters. In *Proceedings of the First Eurographics Conference on Sketch-Based Interfaces and Modeling (SBM'04)*. Eurographics Association, Aire-la-Ville, Switzerland, Switzerland, 175–182. <https://doi.org/10.2312/SBM/SBM04/175-182>
- Lingjing Wang, Cheng Qian, Jifei Wang, and Yi Fang. 2018a. Unsupervised Learning of 3D Model Reconstruction from Hand-Drawn Sketches. (2018), 1820–1828. <https://doi.org/10.1145/3240508.3240699>
- Peng-Shuai Wang, Yang Liu, Yu-Xiao Guo, Chun-Yu Sun, and Xin Tong. 2017. O-CNN: Octree-based Convolutional Neural Networks for 3D Shape Analysis. *ACM Trans. Graph.* 36, 4, Article 72 (July 2017), 11 pages. <https://doi.org/10.1145/3072959.3073608>
- Shaoxiong Wang, Jiajun Wu, Xingyuan Sun, Wenzhen Yuan, William T Freeman, Joshua B Tenenbaum, and Edward H Adelson. 2018b. 3D Shape Perception from Monocular Vision, Touch, and Shape Priors. In *IEEE/RSJ International Conference on Intelligent Robots and Systems (IROS)*.
- Weiyue Wang, Duygu Ceylan, Radomir Mech, and Ulrich Neumann. 2019. 3DN: 3D Deformation Network. (2019). arXiv:1903.03322 <http://arxiv.org/abs/1903.03322>
- Francis Williams, Teso Schneider, Claudio Silva, Denis Zorin, Joan Bruna, and Daniele Panozzo. 2018. Deep Geometric Prior for Surface Reconstruction. (2018). <https://doi.org/10.1109/ICCV.2018.00093> arXiv:1811.10943v1 arXiv:1811.10943
- Jiajun Wu, Yifan Wang, Tianfan Xue, Xingyuan Sun, William T. Freeman, and Joshua B. Tenenbaum. 2017. MarrNet: 3D Shape Reconstruction via 2.5D Sketches. *Nips* (2017). arXiv:1711.03129 <http://arxiv.org/abs/1711.03129>
- Jiajun Wu, Tianfan Xue, Joseph J. Lim, Yuandong Tian, Joshua B. Tenenbaum, Antonio Torralba, and William T. Freeman. 2016a. Single image 3D interpreter network. *Lecture Notes in Computer Science (including subseries Lecture Notes in Artificial Intelligence and Lecture Notes in Bioinformatics)* 9910 LNCS (2016), 365–382. https://doi.org/10.1007/978-3-319-46466-4_22 arXiv:arXiv:1604.08685v2
- Jiajun Wu, Chengkai Zhang, Tianfan Xue, William T. Freeman, and Joshua B. Tenenbaum. 2016b. Learning a Probabilistic Latent Space of Object Shapes via 3D Generative-Adversarial Modeling. *Nips* (2016). arXiv:1610.07584 <http://arxiv.org/abs/1610.07584>
- Jiajun Wu, Chengkai Zhang, Xiuming Zhang, Zhoutong Zhang, William T Freeman, and Joshua B Tenenbaum. 2018. Learning 3D Shape Priors for Shape Completion and Reconstruction. In *European Conference on Computer Vision (ECCV)*.
- Baoxuan Xu, William Chang, Alla Sheffer, Adrien Bousseau, James McCrae, and Karan Singh. 2014. True2Form. *ACM Transactions on Graphics* 33, 4 (2014), 1–13. <https://doi.org/10.1145/2601097.2601128>
- Xinchen Yan, Jimei Yang, Ersin Yumer, Yijie Guo, and Honglak Lee. 2016. Perspective Transformer Nets: Learning Single-View 3D Object Reconstruction without 3D Supervision. *d. Nips* (2016), 1–15. arXiv:1612.00814 <http://arxiv.org/abs/1612.00814>
- Linjie Yang, Jianzhuang Liu, and Xiaoou Tang. 2013. Complex 3D general object reconstruction from line drawings. *Proceedings of the IEEE International Conference on Computer Vision* (2013), 1433–1440. <https://doi.org/10.1109/ICCV.2013.181>
- Yaoqing Yang, Chen Feng, Yiru Shen, and Dong Tian. 2018. FoldingNet: Point Cloud Auto-Encoder via Deep Grid Deformation. In *The IEEE Conference on Computer Vision and Pattern Recognition (CVPR)*.
- Fisher Yu and Vladlen Koltun. 2016. Multi-Scale Context Aggregation by Dilated Convolutions. *ICLR* (2016).
- Xiuming Zhang, Zhoutong Zhang, Chengkai Zhang, Joshua B Tenenbaum, William T Freeman, and Jiajun Wu. 2018. Learning to Reconstruct Shapes from Unseen Classes. In *Advances in Neural Information Processing Systems (NeurIPS)*.
- Zhirong Wu, S. Song, A. Khosla, Fisher Yu, Linguang Zhang, Xiaoou Tang, and J. Xiao. 2015. 3D ShapeNets: A deep representation for volumetric shapes. In *2015 IEEE Conference on Computer Vision and Pattern Recognition (CVPR)*. 1912–1920. <https://doi.org/10.1109/CVPR.2015.7298801>
- L. Zhu, T. Igarashi, and J. Mitani. 2013. Soft Folding. *Computer Graphics Forum* 32, 7 (2013), 167–176. <https://doi.org/10.1111/cgf.12224> arXiv:<https://onlinelibrary.wiley.com/doi/pdf/10.1111/cgf.12224>
- Chuhang Zou, Ersin Yumer, Jimei Yang, Duygu Ceylan, and Derek Hoiem. 2017. 3D-PRNN: Generating Shape Primitives with Recurrent Neural Networks. *CoRR* abs/1708.01648 (2017). arXiv:1708.01648 <http://arxiv.org/abs/1708.01648>